UC Irvine

UC Irvine Previously Published Works

Title

Composite Bijel-Templated Hydrogels for Cell Delivery

Permalink

https://escholarship.org/uc/item/8kt0b92r

Journal

ACS Biomaterials Science & Engineering, 4(2)

ISSN

2373-9878

Authors

Thorson, Todd J

Botvinick, Elliot L

Mohraz, Ali

Publication Date

2018-02-12

DOI

10.1021/acsbiomaterials.7b00809

Peer reviewed

eScholarship.org Powered by the California Digital Library
University of California

Author Manuscript

Author Manuscript

Author Manuscript

Author Manuscript

HHS Public Access

Author manuscript

ACS Biomater Sci Eng. Author manuscript; available in PMC 2018 December 14.

Published in final edited form as:

ACS Biomater Sci Eng. 2018 February 12; 4(2): 587–594. doi:10.1021/acsbiomaterials.7b00809.

Composite bijel-templated hydrogels for cell delivery

Todd J. Thorson[a], **Elliot L. Botvinick**[b,*], and **Ali Mohraz**[a,*]

[a]Department of Chemical Engineering and Materials Science, University of California, Irvine, CA 92697, USA

[b]Department of Biomedical Engineering, University of California, Irvine, CA 92697, USA

Abstract

Numerous processing techniques aim to impart interconnected, porous structures within regenerative medicine materials to support cell delivery and direct tissue growth. Many of these techniques lack predictable control of scaffold architecture, and rapid prototyping methods are often limited by time-consuming, layer-by-layer fabrication of micro-features. Bicontinuous interfacially jammed emulsion gels (bijels) offer a robust, self-assembly-based platform for synthesizing a new class of morphologically unique cell delivery biomaterials. Bijels form *via* kinetic arrest of temperature-driven spinodal decomposition in partially miscible binary liquid systems. These non-equilibrium soft materials are comprised of co-continuous, fully percolating, non-constricting liquid domains separated by a nanoparticle monolayer. Through the selective introduction of biocompatible precursors, hydrogel scaffolds displaying the morphological characteristics of the parent bijel can be formed. We report using bijel templating to generate structurally unique, fibrin-loaded polyethylene glycol hydrogel composites. Demonstration of composite bijel-templated hydrogels (CBiTHs) as a new cell delivery system was carried out *in vitro* using fluorescence-based tracking of cells delivered to previously acellular fibrin gels. Imaging analysis confirmed repeatable delivery of normal human dermal fibroblasts to acellular fibrin gels.

Keywords

bijel; self-assembly; cell delivery; composite; microstructure

1. Introduction

Hydrogels have been extensively explored as regenerative biomaterials that offer tunability of surface chemistry, stiffness, and degradability while providing a cross-linked matrix that mimics native tissue environments.[1,2] Hydrogels of both natural and synthetic origin have been widely used as regenerative medicine materials.[3–5] Fibrin, a natural origin hydrogel formed as a result of the thrombosis cascade, provides an attractive bio-mimetic extracellular matrix for cell delivery.[6–8] However, weak mechanical properties complicate implantation, and natural forces encountered within the body may undesirably deform fibrin during *in situ*

*Corresponding Authors: elliot.botvinick@uci.edu, mohraz@uci.edu.

Supporting Information Available: The following files are available free of charge.

Author Manuscript Author Manuscript Author Manuscript Author Manuscript

gelation approaches.[9,10] Conversely, synthetic hydrogels can be used to generate mechanically robust cell encapsulation matrices using a variety of processing conditions, but they do not provide a viable fibrous three dimensional (3D) extracellular matrix (ECM) mimic for cell attachment and growth.[11] Numerous strategies have been developed that incorporate natural, cell recognizable motifs in synthetic hydrogels for the fabrication of hybrid biomaterial systems. For instance, Arg-Gly-Asp (RGD) adhesion and matrix metalloproteinase (MMP) degradation sites have been incorporated into synthetic polymers for increased control of cell viability and differentiation.[12–15] While these hybrid approaches enable more functional cell encapsulation materials, cells do not experience a completely natural fiber matrix for phenotype preservation, and transport of cell metabolites and waste is often limited. A composite system that selectively offers the advantages of an unmodified, natural encapsulation hydrogel and a synthetic support scaffold can aid in overcoming drawbacks experienced in current cell delivery strategies.[16]

One inherent advantage of using hydrogels in regenerative medicine is the flexibility offered in processing conditions, permitting the creation of microporous scaffolds containing interconnected pore networks for enhanced proliferation, migration, and transport pathways.[17,18] Common processing techniques for generating porous hydrogels include porogen templating of particles[16,19], ice[20,21], and salt[22,23], high internal phase emulsion (HIPE) polymerization[24,25], electrospinning[26,27], and projection stereolithography (PSL).[28,29] While porogen templating, HIPE polymerization, and other process-based techniques are able to readily generate porosity in scaffolds, precise control of the entire architecture is often limited with these techniques. The result is typically a random pore morphology that can lead to unreliable loading of cells and therapeutics, underutilized scaffold surface area, unpredictable mechanical properties, and constricted transport pathways. Rapid prototyping methods such as PSL offer layer-by-layer construction of rationally designed biomaterial architectures.[30] Such techniques are able to generate arbitrarily complex scaffolds that exhibit enhanced transport and mechanical properties. Examples include porous constructs based on minimal surface models (*e.g.* Schwarz D, Schoen's G) marked by periodic geometric units that form fully interconnected, co-continuous solid-void phases.[28] However, using layer-by-layer techniques to fabricate features with micro-scale resolution remains inefficient, rendering scale-up processing impractical.[29,31]

Herein, we report a self-assembly-based processing technique for the generation of morphologically unique hydrogel composites comprised of fully interconnected bicontinuous phases with uniform and tunable pore sizes. We demonstrate the utility of our composites as mechanically robust cell delivery systems that enable uninhibited delivery in a natural environment. Bicontinuous interfacially jammed emulsion gels (bijels) are a new class of non-equilibrium soft materials first proposed *via* simulations in 2005[32] and realized experimentally in 2007.[33,34] Bijels are formed by colloidal particle self-assembly and kinetic arrest of spinodal decomposition in partially miscible binary solutions. Spinodal decomposition prompts widespread coarsening of the fluid-fluid interface when the system is quenched at its critical composition. Particles with equal affinity for the two fluid phases strongly adsorb at the interface during phase separation. Phase separation is kinetically arrested once the interfacial area is fully occupied by particles, and the mixture undergoes a sharp gelation transition (Figure 1a–c).[35,36] Bijels exhibit predictable morphological

Author Manuscript Author Manuscript Author Manuscript Author Manuscript

attributes distinguished by bicontinuous, fully interpenetrating, non-constricting microchannels separated by a nanoparticle monolayer.[34] Furthermore, the self-assembly of bijels driven by spinodal decomposition naturally forms a minimal surface geometry marked by uniform domain size, negative Gaussian curvature and vanishing mean curvature. These unique features culminate to form an internal architecture with saddle points at the majority of internal surface sites.[37] Finally, control of the characteristic domain size, x_i, within the range 5 μm < x_i < 800 μm, is afforded through particle loading, where higher particle volume fractions arrest spinodal decomposition at an earlier stage, resulting in a smaller domain size, and *vice versa*.[33,38]

Lee and Mohraz demonstrated in 2010 that bijels could serve as robust templates for fabrication of microporous materials containing the inherent morphological features of the parent bijel.[39] Extending these techniques, the present study utilizes bijels for the template-based synthesis of porous polyethylene glycol (PEG) scaffolds with spinodal-like microstructure, in which the domain size is specifically tuned to facilitate robust cell loading and migration, uninhibited by pore-to-pore constrictions present in porogen-templated biomaterials.[16] Composite bijel-templated hydrogels (CBiTHs) are then synthesized by filling the interconnected micro-channel network inside the PEG scaffold with a cell-encapsulating fibrin matrix. CBiTHs combine the advantages of natural and synthetic hydrogels, enabling a mechanically robust material in which a natural 3D ECM phase is present and readily accessible throughout the volume. The utility of CBiTHs as cell delivery systems is demonstrated through tracking of normal human dermal fibroblast (NHDF) loading and delivery to initially-acellular surrounding fibrin gels.

2. Materials and Methods

2.1. Materials

All reagents and materials were used as received. Rhodamine B isothiocyanate (RITC), tetraethyl orthosilicate (TEOS), 2,6-lutidine, poly(ethylene glycol) diacrylate (PEGDA; number average molecular weight (M_n): 258 g mol^{-1}), protamine sulfate, thrombin from bovine plasma, formalin solution (neutral buffered, 10%), bovine serum albumin, and fluorescein isothiocyanate-dextran (average molecular weight: 150 kDa) were purchased from Sigma-Aldrich (St. Louis, MO, USA). (3-aminopropyl) triethoxysilane (APTES) was purchased from TCI America (Portland, OR, USA). Poly(dimethylsiloxane) (PDMS) was purchased from Dow Corning (Auburn, MI, USA). 2-hydroxy-2-methylpropiophenone photoinitiator (Darocur 1173) was obtained from Ciba Specialty Chemicals (Tarrytown, NY, USA). Ammonium hydroxide (Fisher Chemical), Dulbecco's modified eagle's medium (DMEM, Gibco), fetal bovine serum (Gibco), penicillin streptomycin (Gibco), phosphate buffered saline (PBS, Gibco), Alexa Fluor 488 fibrinogen (Invitrogen), Alexa Fluor 488 phalloidin (Invitrogen), 4',6-diamidino-2-phenylindole, dihydrochloride (DAPI, Invitrogen), and Triton-100× (Arcos Organics) were purchased from Thermo Fisher Scientific (Waltham, MA, USA). Green fluorescent protein reporter plasmid (QM511B-1, Systems Biosciences, Palo Alto, CA, USA) and lentivirus titer were generously supplied by Professor Timothy Downing (UC, Irvine). Ultraviolet (UV)-curable adhesive was purchased from Norland Products (NOA 61, Cranbury, NJ, USA).

Author Manuscript Author Manuscript Author Manuscript Author Manuscript

2.2. Preparation of bijel-templated hydrogel scaffolds

Bijels were used as the template platform for synthesizing polyethylene glycol (PEG) scaffolds. Fluorescently modified silica nanoparticles (500 nm) were synthesized following an adapted Stöber process.[40] First, RITC was coupled to APTES by mixing 12.5 mg RITC and 24.9 mg APTES in 10 mL of ethanol at room temperature overnight. The resulting dye solution was split into two flasks containing 4.18 mL TEOS, 10 mL ammonium hydroxide solution, and 56 mL ethanol and continuously stirred overnight. Silica nanoparticles were washed with deionized water and pelleted *via* centrifugation (12 minutes, 2500 rpm) three times and dried under vacuum at 135°C until neutrally wetting surface chemistry was observed. Nanoparticle wetting properties were tracked using an inverted microscope coupled to a Vt-eye confocal scanner (VisiTech International, Sunderland, UK). Bijels were formed by dispersing 1% (*v/v*) silica nanoparticles in a critical mixture of Milli-Q water and 2,6-lutidine (x_{Lut} = 0.064) using a Branson Sonifier 250 (Emerson, St. Louis, MO, USA). The mixture was transferred to a custom-assembled vessel comprised of a cylindrical glass tube (5 mm inner diameter) oriented vertically on a microscope coverslip using PDMS as a bonding agent between the two glass components (Figure 1a). Microwave heating was supplied to initiate spinodal decomposition and bijel formation (Figure 1b). Bijels were allowed to stabilize for 10 minutes in an oven maintained at 70°C. A hydrogel precursor solution of PEGDA containing 1% *v/v* Darocur 1173 photoinitiator was chosen to naturally partition into the 2,6-lutidine phase. 35 μL of this solution was gently added to the top surface of the bijel and allowed to diffuse for at least 2 hours at 70°C (Figure 1c). Radical polymerization of the PEGDA-loaded 2,6-lutidine phase was performed using a UV lamp (Lumen Dynamics, Mississauga, On, Canada; wavelength: 300–500nm) for a period of 100 seconds, thereby locking the templated structure in place (Figure 1d). PEG scaffolds were removed from the glass vessels, rinsed twice with isopropyl alcohol, and allowed to dry uncovered at room temperature overnight.

2.3. Cell culture

Adult normal human dermal fibroblasts (NHDFs) were obtained from Lonza (CC-2511, Walkersville, MD, USA) and cultured at 37°C under air supply containing 5% carbon dioxide (CO_2). DMEM containing 10% fetal bovine serum and 1% penicillin streptomycin was used as the culture medium. Cells were grown to 90% confluency before passaging. Passage numbers no greater than 8 were used for all testing.

2.4. GFP expression in NHDFs

Green fluorescent protein (GFP) expression was used for live tracking of NHDFs during all experiments. GFP expression was achieved through transduction using a QM511B-1 plasmid with a GFP reporter and EF-1α promoter sequence. The plasmid was packaged in lentivirus particles. NHDFs (passage number 4) were seeded into a 12-well plate at a concentration of 150,000 cells/well. Culture medium (1 mL) supplemented with the lentivirus titer and protamine (7μg/mL) was added to each well and cultured for 48 hours to achieve a transduction efficiency of at least 90%.

Author Manuscript Author Manuscript Author Manuscript Author Manuscript

2.5. Fibrin and NHDF loading in bijel-templated scaffolds

NHDFs were trypsinized and re-suspended in 2.5 mg/mL bovine fibrinogen solution at a concentration of 1 million cells/mL for all loading experiments. For sterilization, bijel-templated PEG scaffolds were irradiated under UV light for 15 minutes, soaked for 5 minutes in a 70% ethyl alcohol solution, and soaked for 5 minutes in fresh PBS (×3). Fluorescently labeled fibrin was obtained by supplementing the fibrinogen solution with 5% (*w/w*) Alexa Fluor 488 fibrinogen. PEG scaffolds were cut into disks (3 mm diameter, 2 mm height) and dried in an oven maintained at 80°C. After drying, disks were placed on glass-bottom dishes (MatTek, Ashland, MA, USA) and pre-wetted with 10 μL PBS. 100 μL of the cell-loaded fibrinogen solution was mixed with thrombin (1 U/mL) by gentle pipet mixing in a micro-centrifuge tube on ice. The resulting mixture was pipetted into the disks by placing the pipet tip gently on the middle section of the top surface of the disk and slowly ejecting the fluid. Fibrin gelation occurred over 30 minutes to yield NHDF-loaded CBiTHs. Culture medium was added and the CBiTH dishes were incubated at 37°C under 5% CO_2 air supply. Control fibrin gels were plated on separate glass-bottom dishes for each experiment.

2.6. Cell delivery to acellular fibrin gels

NHDF-loaded CBiTHs were allowed to stabilize for one hour under normal incubation conditions. For delivery to acellular fibrin gels, a biopsy punch with an inner diameter of 2 mm was used to cut out cylindrical sections of the CBiTHs. The cut piece was placed onto a new glass-bottom dish and a fresh mixture of fibrinogen and thrombin (2.5 mg/mL and 1 U/mL, respectively) was deposited circumferentially around the transferred piece. The newly deposited fibrin gels were allowed to form for 30 minutes. Culture medium was added and the dishes were returned to incubation conditions (Figure 2).

2.7. Time-lapse tracking of NHDF delivery

Confocal microscopy imaging was performed at 2 day intervals for a total of 8 days using a FluoView 1200 laser confocal scanning system (Olympus, Center Vally, PA, USA). Pixel density per area was used to report cell density in all experiments, and MATLAB (MathWorks, Natick, MA, USA) was used for image processing. Portable network graphics (PNG) images were read into MATLAB and passed through the multilevel threshold function “multithresh.” The dimmest pixel class, Class 1, was excluded for all subsequent processing. Pixel density, ϕ, was defined as the fraction of class 2 and 3 pixels at each radial distance beginning at the CBiTH-acellular fibrin interface. At each time point, ϕ was evaluated and total bright pixels outside the CBiTH were counted (n=3). At the conclusion of the experiment, all samples were fixed with 10% formalin solution, permeabilized with 0.1% (*v/v*) Triton-100× in PBS, and blocked with 2% bovine serum albumin. F-actin fibrils were stained with Alexa Fluor 488 phalloidin, and nuclei were stained with DAPI for fluorescence confocal microscopy.

2.8. Diffusion of dextran in bijel-templated PEG scaffolds

Diffusion of a fluorescein isothiocyanate-conjugated dextran in bijel-templated PEG scaffolds was measured *via* time-lapse fluorescent imaging using the FluoView 1200 confocal system. Each sample (2 mm height, 1048 μm radius) was soaked in PBS for one

Author Manuscript Author Manuscript Author Manuscript Author Manuscript

hour and placed axially on a glass-bottom dish. A glass coverslip was then attached to the top of each sample using UV-curable optical adhesive. A dextran solution (500 μL, 5 mg/mL PBS) was loaded into the dish and images were captured under 4× magnification every 30 seconds for 60 minutes. Acquired images were then processed in MATLAB to calculate average pixel intensity per radial bin (Δr=57.58 μm). Normalized intensity was calculated by dividing average pixel intensity per bin by the average pixel intensity outside the sample. The experimental data generated from 3 separate samples were fit to a model of transient radial diffusion in cylindrical coordinates. Applying a constant-concentration boundary condition, the theoretical solution used for this model is shown in Equation 1:

$$\frac{c}{c_0} = 2\beta \sum_{n=1}^{\infty} \frac{J_0\left(\frac{\lambda_n r}{R}\right)\left[1 - exp\left(\frac{\lambda_n^2 D_e t}{R^2}\right)\right]}{\lambda_n J_1(\lambda_n)} \quad (1)$$

where r is the radial position; t is the time; R is the sample radius; D_e is the effective diffusivity of dextran in the scaffold; $\beta < 1$ accounts for the void phase of the sample available for dextran diffusion; J_0 and J_1 are Bessel functions of the first kind of zeroth and first order, respectively; and λ_n are the eigenvalues corresponding to solutions of $J_0(\lambda_n)=0$. Assuming average intensity is proportional to the local concentration, adjustable parameters β and D_e were extracted by fitting experimental average intensity data to the model using non-linear least-squared regression with 3000 terms in the series.

2.9. Mechanical testing

Compression tests were performed using a MTS Synergie 100 mechanical tester (MTS Systems, Eden Prairie, MN, USA). Control PEG hydrogels containing no microstructural features were prepared by UV polymerization of the PEGDA and Darocur 1173 solution (36.2% *v/v*) in 2,6-lutidine in the custom-assembled cylindrical glass vessels. Samples of control PEG, bijel-templated PEG, and fibrin-loaded PEG CBiTHs were cut into cylindrical disks (2 mm height, 2 mm diameter) using a razor blade and a biopsy punch. All samples were hydrated in PBS for at least 1 hour before testing (n=3). The cylindrical disks were placed onto the Synergie 100 stage and the compression adapter was lowered to the sample gap height of 2 mm. TestWorks4 (MTS Systems) was used to acquire data during compression to 50% of the sample height. Stress (σ) was plotted versus strain (ε), and the slope of the initial linear region was calculated using linear regression and reported as the sample's compressive modulus (E). The stress at each sample's failure point was reported as the compressive strength (σ_u).

2.10. Statistical analysis

Two-sample, non-paired t-tests were performed in OriginPro (OriginLab, Northampton, MA, USA) for compression testing using the Bonferroni correction (3 comparison groups). Results were considered statistically significant when $p < 0.0167$.

Author Manuscript Author Manuscript Author Manuscript Author Manuscript

3. Results

3.1. Fibrin and NHDF loading in bijel-templated PEG scaffolds

The feasibility of loading a natural hydrogel within the bijel-templated PEG scaffold was tested using fluorescently labeled fibrinogen followed by laser scanning confocal microscopy. A fibrous network microstructurally similar to control gels indicated that fibrinogen was uniformly loaded and homogeneously cross-linked within the interconnected void of the bijel-templated PEG scaffold, resulting in a hydrogel composite with bicontinuous, spinodal-like arrangement of its constituent PEG and fibrin phases (Figure 3a–b). In the next experiment, NHDFs were added to the fibrinogen/thrombin solution and loaded in bijel-templated PEG scaffolds. NHDFs displayed spread phenotypes within the CBiTH after 8 days in culture (Figure 3c).

3.2. Cell delivery to acellular fibrin gels

Cell delivery of NHDFs to acellular fibrin gels was demonstrated using the biopsy punch technique described above (Section 2.6, Figure 2). Confocal microscopy performed at 2 day intervals over the span of 8 days showed that NHDFs loaded within hydrogel composite materials were able to migrate to the surrounding fibrin gels (Figure 4a; additional examples found in supporting information, Figure S1). Quantitative tracking showed the development of a radial gradient in the cell population (bright pixel density), which increased over time indicating cell migration outside of the CBiTH boundary (Figure 4b). Taken as a whole, tracking of cell populations in the surrounding fibrin gels indicated the total cell density increased over time (Figure 4c). Active migration of NHDFs was directly observed *via* time-lapse fluorescent imaging. A video of active migration is supplied as supporting information. NHDFs were observed migrating within the fibrin-filled pores of the composite and moving into the surrounding fibrin gels over the course of 20 hours. In addition, NHDFs fixed and stained 8 days post-transfer were observed spreading within the fibrin phase of the CBiTHs, extending through pores at the boundary, and populating the previously acellular fibrin gels (Figure 5a). Confocal microscopy at increased magnification captured NHDFs at the CBiTH boundary in intimate contact with the surrounding fibrin matrix to further confirm cell delivery using the described *in vitro* delivery methods (Figure 5b).

3.3. Diffusion of dextran in bijel-templated PEG scaffolds

The experimental results and fitting results of the transient radial diffusion model (Equation 1) for 5 radial locations are shown in Figure 6a. The model fits (solid lines) show good agreement with experimental data (open symbols) with extracted parameters of D_e=5.06E-7 cm^2s^{-1} ± 15.45% and β=0.84. A video showing the dynamics of dextran diffusion is supplied as supporting information, and a confocal micrograph after overnight incubation in the dextran solution is shown in Figure 6b. Dextran, represented by fluorescence signal, was present in approximately 50% of the scaffold (supporting information Figure S2).

3.4. Mechanical testing

The mean compressive modulus and strength for control, bijel-templated, and fibrin-loaded bijel-templated (CBiTH) PEG samples are presented in Table 1. Control PEG specimens

Author Manuscript Author Manuscript Author Manuscript Author Manuscript

exhibited the greatest compressive modulus, as expected of the bulk material. Incorporation of the porous microchannel network resulting from bijel-templating decreased the compressive modulus of bijel-templated PEG scaffolds relative to controls. Fibrin loading in CBiTHs resulted in a slight increase in compressive modulus, compared to the porous PEG scaffold. No statistically significant differences were observed between bijel-templated and CBiTH compressive moduli measurements. Additionally, no statistically significant differences were observed between compressive strength measurements across all sample types.

4. Discussion

We have successfully fabricated composite systems that combine discrete phases of natural and synthetic hydrogels at characteristic length scales relevant to cell loading and migration. Our CBiTHs are comprised of a PEG scaffold which provides a mechanically robust backbone, and a sample-spanning fibrin phase which provides a natural fibrous ECM environment for cell encapsulation. The combinatorial advantages of these composites as cell delivery systems are showcased in the present study using CBiTHs to deliver NHDFs to an acellular fibrin gel *in vitro*. CBiTHs are structured such that cell loading is achieved uniformly throughout the entire volume, and uniform pore morphology may aid in a milder loading condition in which cells are not subjected to high shear stresses encountered in a random pore morphology. Once loaded, cells exhibit a similar morphology to those encapsulated in control fibrin gels, able to spread in a 3D ECM. The non-constricting, fully percolating microchannel network inside the composite provides ample routes for metabolite transport and allows uninhibited albeit tortuous pathways for cell migration throughout the volume and out of the composite. To further investigate the microchannel network present in bijel-templated PEG scaffolds, a fluorescence-based diffusion analysis was performed using a simple model for transient diffusion. The model fits show good agreement with experimental data. The effective diffusivity extracted from modeling (5.06E-7 cm^2s^{-1}) was comparable to the expected free diffusion of 150 kDa dextran calculated using the Stokes-Einstein equation (3.65E-7 cm^2s^{-1}).[41] The plateau intensity (β=0.84) was greater than the void fraction calculated by thresholding at steady state (Ω=0.502), which can be explained as follows. The axial resolution of confocal imaging (58 μm as calculated using a numerical aperture of 0.13, wavelength of 488nm, and refractive index of 1)[42] is larger than the domain size in the CBiTH. Therefore, light collected at each pixel will include out of focus fluorescence from regions above and below. Consequently, the solid scaffold regions will not appear completely dark and $\beta > \Omega$.

CBiTHs can be cut, picked up, and transferred without damaging the structure of its hydrogel phases. In this work, we have demonstrated that NHDFs may be seeded in fibrin within the PEG scaffold, moved to a new dish without damage to the composite, and delivered to acellular fibrin in a repeatable fashion. NHDF migration from the CBiTH to the surrounding fibrin clot, captured extensively through time-resolved imaging, indicates that moving the CBiTH sample does not induce significant damage to the cell-encapsulating fibrin matrix. Bijel templates are readily generated through a simple temperature quench. These self-assembled templates, comprised of bicontinuous, fully interpenetrating microscale domains separated by a monolayer of particles, offer a new route to scalable cell

Author Manuscript Author Manuscript Author Manuscript Author Manuscript

delivery systems. Bijel templating can be readily expanded to a larger library of biocompatible hydrogel precursors, with the sole requirement being selective miscibility and preferred partitioning into one of the bijel liquid phases. In the present study, PEG-based CBiTHs were not designed to degrade. However, the bijel templating process can be modified to incorporate hydrolytically and enzymatically degradable moieties to synthesize PEG hydrogels with desired degradation profiles.[43–45] Additionally, silica nanoparticles containing the conjugated RITC fluorophore remain imbedded at the bijel-templated PEG scaffold surface and provide fluorescence during cell tracking experiments. In further designs for cell delivery *in vivo* using CBiTHs, these nanoparticles can be removed prior to cell loading through additional processing with hydrofluoric acid as demonstrated in supporting information (Figure S3).

5. Conclusions

We report a self-assembly-based synthesis method for a new class of cell delivery composite hydrogels. Bijels afford a robust platform for synthesis of biomaterials containing co-continuous, fully interpenetrating, non-constricting void/polymer phases displaying near-minimal surface geometry. Through fluorescence-based tracking of NHDF migration into acellular fibrin hydrogels, we have demonstrated the utility of CBiTHs as cell delivery systems comprised of a synthetic PEG scaffold and a natural fibrin seeding matrix. Active migration of NHDFs from CBiTHs was captured *via* fluorescence microscopy. Image analysis confirmed radial cell density growth in surrounding fibrin over the course of 8 days demonstrating cell delivery in a repeatable fashion.

Supplementary Material

Refer to Web version on PubMed Central for supplementary material.

Acknowledgments

We acknowledge Professor Timothy Downing for providing the plasmid and lentivirus used as a GFP reporter, and Linda McCarthy for performing the NHDF transduction. This work was supported by the NASA Research Opportunities in Complex Fluids and Macromolecular Biophysics Program (NNX13AQ69G) and the National Institutes of Health Laser Microbeam and Medical Program (P41EB015890). T.J.T. acknowledges the National Science Foundation Interdisciplinary Graduate Education and Research Traineeship (IGERT) Biophotonics across Energy, Space, and Time (BEST) program for financial support and training (NSF-DGE-1144901).

References

1. Peppas NA, Hilt JZ, Khademhosseini A, Langer R. Hydrogels in Biology and Medicine: From Molecular Principles to Bionanotechnology. Adv. Mater. 2006; 18:1345–1360. DOI: 10.1002/adma.200501612
2. Buwalda SJ, Boere KWM, Dijkstra PJ, Feijen J, Vermonden T, Hennink WE. Hydrogels in a Historical Perspective: From Simple Networks to Smart Materials. J. Controlled Release. 2014; 190:254–273. DOI: 10.1016/j.jconrel.2014.03.052
3. Ozdil D, Aydin HM. Polymers for Medical and Tissue Engineering Applications. J. Chem. Technol. Biotechnol. 2014; 89:1793–1810. DOI: 10.1002/jctb.4505
4. Patterson J, Martino MM, Hubbell JA. Biomimetic Materials in Tissue Engineering. Mater. Today. 2010; 13:14–22. DOI: 10.1016/S1369-7021(10)70013-4

Author Manuscript Author Manuscript Author Manuscript Author Manuscript

5. Malafaya PB, Silva GA, Reis RL. Natural–Origin Polymers as Carriers and Scaffolds for Biomolecules and Cell Delivery in Tissue Engineering Applications. Adv. Drug Deliv. Rev. 2007; 59:207–233. DOI: 10.1016/j.addr.2007.03.012 [PubMed: 17482309]
6. Ahmed TAE, Dare EV, Hincke M. Fibrin: A Versatile Scaffold for Tissue Engineering Applications. Tissue Eng. Part B Rev. 2008; 14:199–215. DOI: 10.1089/ten.teb.2007.0435 [PubMed: 18544016]
7. Li Y, Meng H, Liu Y, Lee BP. Fibrin Gel as an Injectable Biodegradable Scaffold and Cell Carrier for Tissue Engineering. Sci. World J. 2015; 2015:685690.doi: 10.1155/2015/685690
8. Brown AC, Barker TH. Fibrin-Based Biomaterials: Modulation of Macroscopic Properties through Rational Design at the Molecular Level. Acta Biomater. 2014; 10:1502–1514. DOI: 10.1016/j.actbio.2013.09.008 [PubMed: 24056097]
9. Zhang G, Wang X, Wang Z, Zhang J, Suggs L. A PEGylated Fibrin Patch for Mesenchymal Stem Cell Delivery. Tissue Eng. 2006; 12:9–19. DOI: 10.1089/ten.2006.12.9 [PubMed: 16499438]
10. Hokugo A, Takamoto T, Tabata Y. Preparation of Hybrid Scaffold from Fibrin and Biodegradable Polymer Fiber. Biomaterials. 2006; 27:61–67. DOI: 10.1016/j.biomaterials.2005.05.030 [PubMed: 16000222]
11. Wang C, Varshney RR, Wang D-A. Therapeutic Cell Delivery and Fate Control in Hydrogels and Hydrogel Hybrids. Adv. Drug Deliv. Rev. 2010; 62:699–710. DOI: 10.1016/j.addr.2010.02.001 [PubMed: 20138940]
12. Benton JA, Fairbanks BD, Anseth KS. Characterization of Valvular Interstitial Cell Function in Three Dimensional Matrix Metalloproteinase Degradable PEG Hydrogels. Biomaterials. 2009; 30:6593–6603. DOI: 10.1016/j.biomaterials.2009.08.031 [PubMed: 19747725]
13. Lutolf MP, Hubbell JA. Synthetic Biomaterials as Instructive Extracellular Microenvironments for Morphogenesis in Tissue Engineering. Nat. Biotechnol. 2005; 23:47–55. DOI: 10.1038/nbt1055 [PubMed: 15637621]
14. Kraehenbuehl TP, Ferreira LS, Zammaretti P, Hubbell JA, Langer R. Cell-Responsive Hydrogel for Encapsulation of Vascular Cells. Biomaterials. 2009; 30:4318–4324. DOI: 10.1016/j.biomaterials.2009.04.057 [PubMed: 19500842]
15. Kim JP, Kong YM, Niedzielski SK, Singh RJ, Putnam A, Shikanov A. Characterization of the Crosslinking Kinetics of Multi-arm Poly(ethylene glycol) Hydrogels Formed via Michael-type Addition. Soft Matter. 2016; 12:2076–2085. DOI: 10.1039/C5SM02668G [PubMed: 26750719]
16. Stachowiak AN, Irvine DJ. Inverse Opal Hydrogel-Collagen Composite Scaffolds as a Supportive Microenvironment for Immune Cell Migration. J. Biomed. Mater. Res. A. 2008; 85A:815–828. DOI: 10.1002/jbm.a.31661
17. Langer R, Tirrell DA. Designing Materials for Biology and Medicine. Nature. 2004; 428:487–492. DOI: 10.1038/nature02388 [PubMed: 15057821]
18. Annabi N, Nichol JW, Zhong X, Ji C, Koshy S, Khademhosseini A, Dehghani F. Controlling the Porosity and Microarchitecture of Hydrogels for Tissue Engineering. Tissue Eng. Part B Rev. 2010; 16:371–383. DOI: 10.1089/ten.teb.2009.0639 [PubMed: 20121414]
19. Choi S-W, Zhang Y, Xia Y. Three-Dimensional Scaffolds for Tissue Engineering: The Importance of Uniformity in Pore Size and Structure. Langmuir. 2010; 26:19001–19006. DOI: 10.1021/la104206h [PubMed: 21090781]
20. Bai H, Polini A, Delattre B, Tomsia AP. Thermoresponsive Composite Hydrogels with Aligned Macroporous Structure by Ice-Templated Assembly. Chem. Mater. 2013; 25:4551–4556. DOI: 10.1021/cm4025827 [PubMed: 24489436]
21. Welzel PB, Grimmer M, Renneberg C, Naujox L, Zschoche S, Freudenberg U, Werner C. Macroporous StarPEG-Heparin Cryogels. Biomacromolecules. 2012; 13(8):2349–2358. DOI: 10.1021/bm300605s [PubMed: 22758219]
22. Jiang B, Waller TM, Larson JC, Appel AA, Brey EM. Fibrin-Loaded Porous Poly(Ethylene Glycol) Hydrogels as Scaffold Materials for Vascularized Tissue Formation. Tissue Eng. Part A. 2012; 19(1–2):224–234. DOI: 10.1089/ten.tea.2012.0120 [PubMed: 23003671]
23. Park JS, Woo DG, Sun BK, Chung H-M, Im SJ, Choi YM, Park K, Huh KM, Park K-H. In Vitro and In Vivo Test of PEG/PCL-Based Hydrogel Scaffold for Cell Delivery Application. J. Controlled Release. 2007; 124:51–59. DOI: 10.1016/j.jconrel.2007.08.030

Author Manuscript Author Manuscript Author Manuscript Author Manuscript

24. Oh BHL, Bismarck A, Chan-Park MB. High Internal Phase Emulsion Templating with Self-Emulsifying and Thermoresponsive Chitosan-graft-PNIPAM-graft-Oligoproline. Biomacromolecules. 2014; 15:1777–1787. DOI: 10.1021/bm500172u [PubMed: 24661070]
25. Nalawade AC, Ghorpade RV, Shadbar S, Shadbar Qureshi M, Chavan NN, Khan AA, Ponrathnam S. Inverse High Internal Phase Emulsion Polymerization (i-HIPE) of GMMA, HEMA and GDMA for the Preparation of Superporous Hydrogels as a Tissue Engineering Scaffold. J. Mater. Chem. B. 2016; 4:450–460. DOI: 10.1039/C5TB01873K
26. Mollet BB, Spaans S, Fard PG, Bax NAM, Bouten CVC, Dankers PYW. Mechanically Robust Electrospun Hydrogel Scaffolds Crosslinked via Supramolecular Interactions. Macromol. Biosci. 2017; 17doi: 10.1002/mabi.201700053
27. Li M, Mondrinos MJ, Chen X, Gandhi MR, Ko FK, Lelkes PI. Co-Electrospun Poly(lactide-co-glycolide), Gelatin, and Elastin Blends for Tissue Engineering Scaffolds. J. Biomed. Mater. Res. A. 2006; 79A:963–973. DOI: 10.1002/jbm.a.30833
28. Gauvin R, Chen Y-C, Lee JW, Soman P, Zorlutuna P, Nichol JW, Bae H, Chen S, Khademhosseini A. Microfabrication of Complex Porous Tissue Engineering Scaffolds using 3D Projection Stereolithography. Biomaterials. 2012; 33:3824–3834. DOI: 10.1016/j.biomaterials.2012.01.048 [PubMed: 22365811]
29. Torres-Rendon JG, Femmer T, De Laporte L, Tigges T, Rahimi K, Gremse F, Zafarnia S, Lederle W, Ifuku S, Wessling M, et al. Bioactive Gyroid Scaffolds Formed by Sacrificial Templating of Nanocellulose and Nanochitin Hydrogels as Instructive Platforms for Biomimetic Tissue Engineering. Adv. Mater. 2015; 27:2989–2995. DOI: 10.1002/adma.201405873 [PubMed: 25833165]
30. Melchels FPW, Bertoldi K, Gabbrielli R, Velders AH, Feijen J, Grijpma DW. Mathematically Defined Tissue Engineering Scaffold Architectures Prepared by Stereolithography. Biomaterials. 2010; 31:6909–6916. DOI: 10.1016/j.biomaterials.2010.05.068 [PubMed: 20579724]
31. Billiet T, Vandenhaute M, Schelfhout J, Van Vlierberghe S, Dubruel P. A Review of Trends and Limitations in Hydrogel-Rapid Prototyping for Tissue Engineering. Biomaterials. 2012; 33:6020–6041. DOI: 10.1016/j.biomaterials.2012.04.050 [PubMed: 22681979]
32. Stratford K, Adhikari R, Pagonabarraga I, Desplat J-C, Cates ME. Colloidal Jamming at Interfaces: A Route to Fluid-Bicontinuous Gels. Science. 2005; 309:2198–2201. DOI: 10.1126/science.1116589 [PubMed: 16195456]
33. Herzig EM, White KA, Schofield AB, Poon WCK, Clegg PS. Bicontinuous Emulsions Stabilized Solely by Colloidal Particles. Nat. Mater. 2007; 6:966–971. DOI: 10.1038/nmat2055 [PubMed: 17982465]
34. Cates ME, Clegg PS. Bijels: A New Class of Soft Materials. Soft Matter. 2008; 4:2132–2138. DOI: 10.1039/B807312K
35. Lee MN, Thijssen JHJ, Witt JA, Clegg PS, Mohraz A. Making a Robust Interfacial Scaffold: Bijel Rheology and its Link to Processability. Adv. Funct. Mater. 2013; 23:417–423. DOI: 10.1002/adfm.201201090
36. Imperiali L, Clasen C, Fransaer JW, Macosko C, Vermant J. A Simple Route Towards Graphene Oxide Frameworks. Mater. Horiz. 2014; 1:139–145. DOI: 10.1039/C3MH00047H
37. Chen H-Y, Kwon Y, Thornton K. Multifunctionality of Three-Dimensional Self-Assembled Composite Structure. Scr. Mater. 2009; 61:52–55. DOI: 10.1016/j.scriptamat.2009.03.006
38. Witt JA, Mumm DR, Mohraz A. Bijel Reinforcement by Droplet Bridging: A Route to Bicontinuous Materials with Large Domains. Soft Matter. 2013; 9:6773–6780. DOI: 10.1039/C3SM00130J
39. Lee MN, Mohraz A. Bicontinuous Macroporous Materials from Bijel Templates. Adv. Mater. 2010; 22:4836–4841. DOI: 10.1002/adma.201001696 [PubMed: 20862712]
40. Van Blaaderen A, Vrij A. Synthesis and Characterization of Colloidal Dispersions of Fluorescent, Monodisperse Silica Spheres. Langmuir. 1992; 8:2921–2931. DOI: 10.1021/la00048a013
41. Larson, R. The Structure and Rheology of Complex Fluids. Oxford University Press Inc; New York, NY: 1999.
42. Inoue, S. Handbook of Biological Confocal Microscopy. Springer Science+Business Media; 2006. Foundations of Confocal Scanned Imaging in Light Microscopy; 1–17.

Author Manuscript Author Manuscript Author Manuscript Author Manuscript

43. Zustiak SP, Leach JB. Hydrolytically Degradable Poly(Ethylene Glycol) Hydrogel Scaffolds with Tunable Degradation and Mechanical Properties. Biomacromolecules. 2010; 11:1348–1357. DOI: 10.1021/bm100137q [PubMed: 20355705]

44. Neumann AJ, Quinn T, Bryant SJ. Nondestructive Evaluation of a New Hydrolytically Degradable and Photo-clickable PEG Hydrogel for Cartilage Tissue Engineering. Acta Biomater. 2016; 39:1–11. DOI: 10.1016/j.actbio.2016.05.015 [PubMed: 27180026]

45. Yu J, Chen F, Wang X, Dong N, Lu C, Yang G, Chen Z. Synthesis and Characterization of MMP Degradable and Maleimide Cross-linked PEG Hydrogels for Tissue Engineering Scaffolds. Polym. Degrad. Stab. 2016; 133:312–320. DOI: 10.1016/j.polymdegradstab.2016.09.008

Author Manuscript Author Manuscript Author Manuscript Author Manuscript

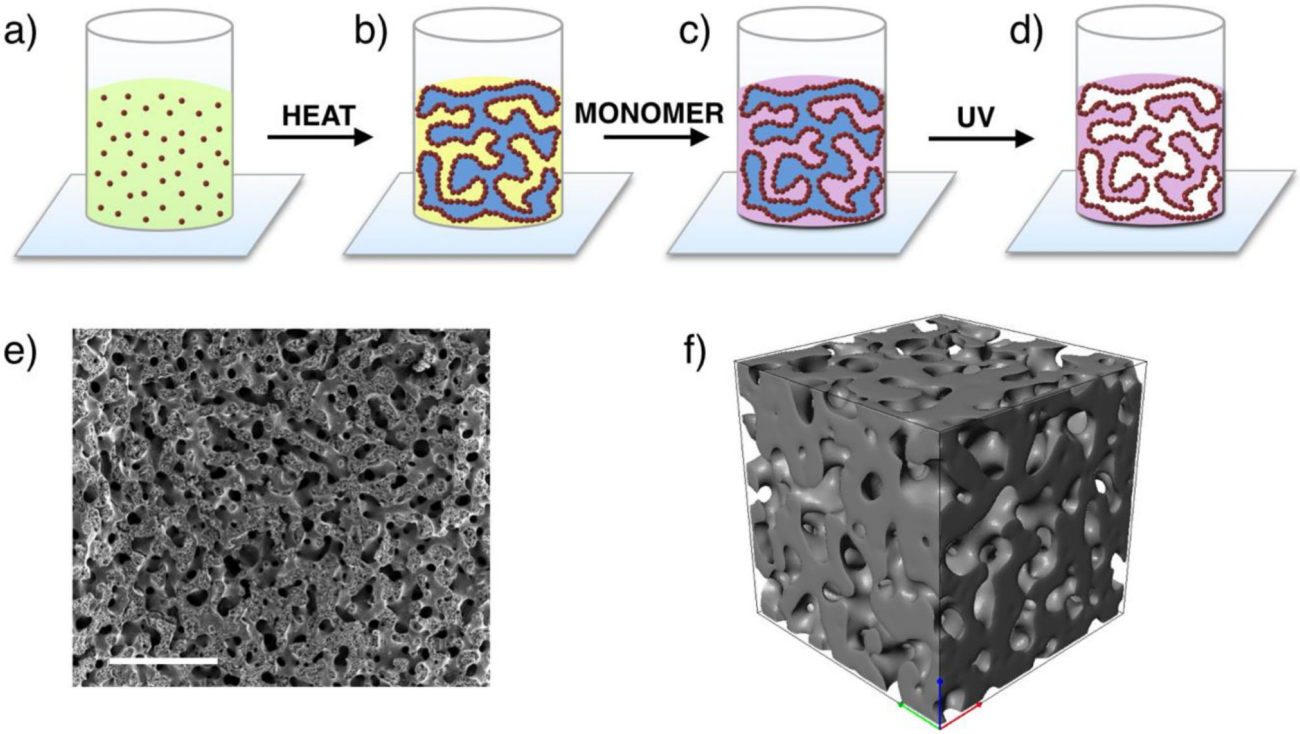

Figure 1.

Bijel-templating process schematic and representative scaffold morphology. a) A mixture of water/2,6-lutidine/silica nanoparticles is loaded into a glass tube. b) The mixture is heated *via* microwaves to trigger spinodal decomposition and subsequent bijel formation as the water/2,6-lutidine interfacial area becomes fully populated by silica nanoparticles. c) PEGDA/Darocur 1173 solution is added to the top surface of the bijel and selectively partitions to the 2,6-lutidine phase. d) UV light initiates radical polymerization and excess liquids are removed from the now bijel-templated scaffold. e) Scanning electron microscopy micrograph (Scale bar: 500 μm) and f) Nano-computed tomography 3D reconstruction of a processed bijel-templated PEG scaffold. Sample imaging details are included in supporting information (S2).

Author Manuscript Author Manuscript Author Manuscript Author Manuscript

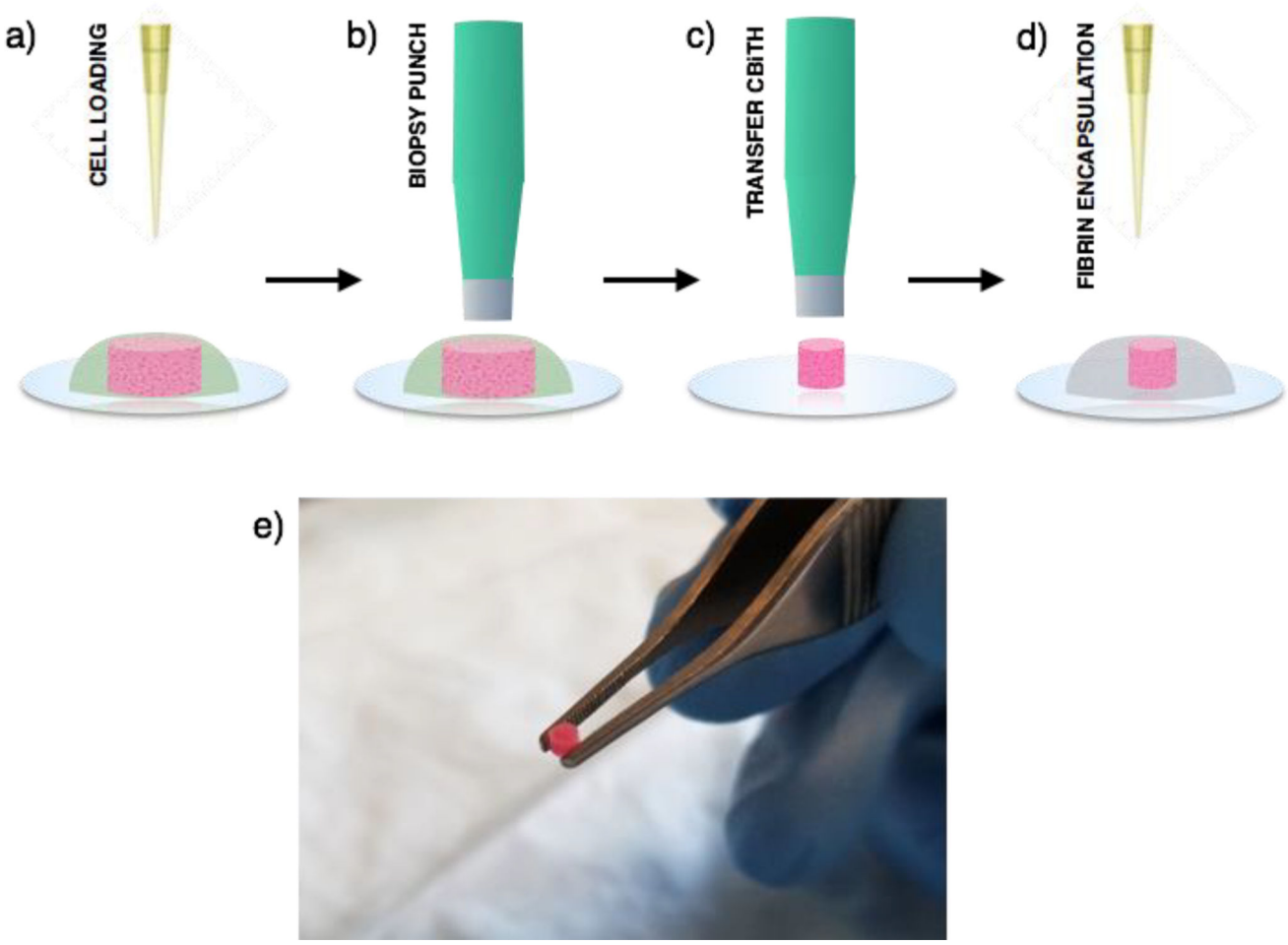

Figure 2.

Cell delivery to acellular fibrin schematic. a) NHDF/fibrinogen/thrombin mixture is injected into the bijel-templated PEG scaffold to form the CBiTH. b) Biopsy punch cuts a cylindrical piece from the NHDF-loaded CBiTH. c) Cut piece is transferred to a fresh incubation dish. d) Fibrinogen/thrombin is added circumferentially around the CBiTH to encapsulate in acellular fibrin. e) CBiTH being held with forceps following biopsy punch.

Author Manuscript Author Manuscript Author Manuscript Author Manuscript

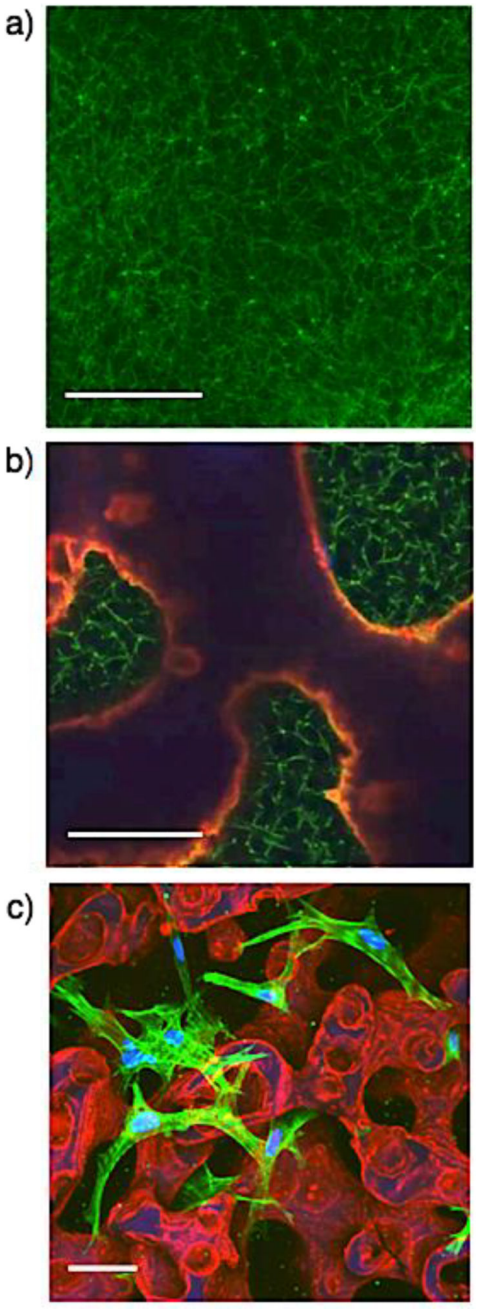

Figure 3.

Fibrin and NHDF loading in bijel-templated PEG scaffolds. a) Confocal micrograph of typical fiber architecture in a fibrin control gel (Green: Alexa Fluor 488 fibrinogen, Scale bar: 50 μm). b) Confocal micrograph of a fibrin-loaded, bijel-templated PEG scaffold (CBiTH) (Green: Alexa Fluor 488 fibrinogen, Red: RITC-labeled silica nanoparticles, Scale bar: 50 μm). c) Confocal microscopy maximum intensity projection (image stack: 155 μm) of a NHDF-loaded CBiTH (Blue: DAPI labeling of cell nuclei, Green: Alexa Fluor 488 phalloidin labeling of F-actin, Red: RITC-labeled silica nanoparticles, Scale bar: 50 μm).

Author Manuscript Author Manuscript Author Manuscript Author Manuscript

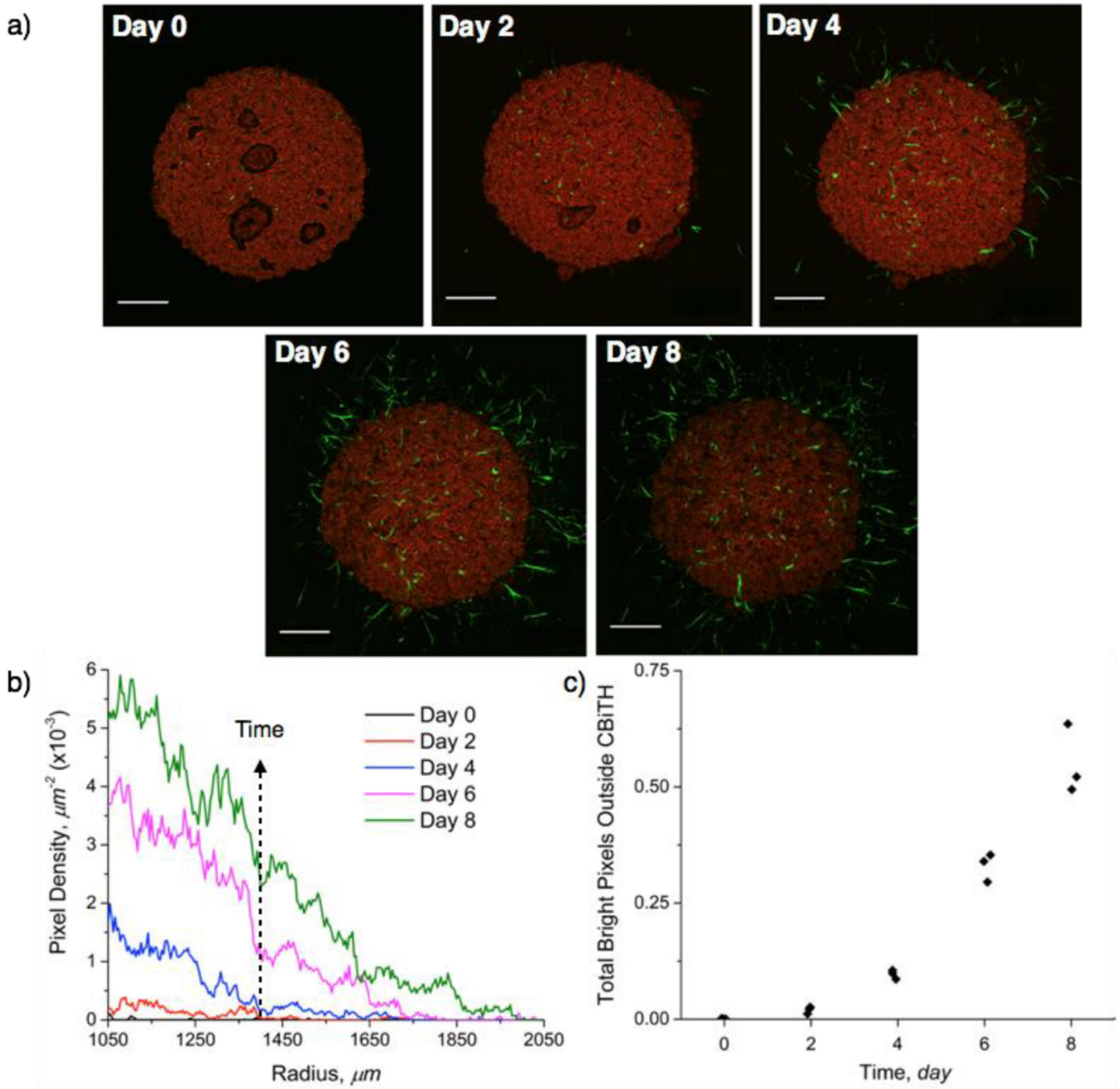

Figure 4.

Time-lapse analysis of cell delivery to acellular fibrin hydrogels using NHDF-loaded CBiTHs. a) Confocal microscopy maximum intensity projections (day 0 image stack: 250 μm, days 2–8 image stack: 750 μm) tracking NHDF delivery over 8 days (Green: GFP expression in NHDFs, Red: RITC-labeled silica nanoparticles, Scale bar: 500 μm). b) Pixel density outside CBiTH boundary (Radius=1050 μm) plotted versus distance (n=3). Line color designations by time: Day 0 (−), Day 2 (−), Day 4 (−), Day 6 (−), Day 8 (−). c) Total bright pixel count outside each CBiTH versus time (n=3).

Author Manuscript Author Manuscript Author Manuscript Author Manuscript

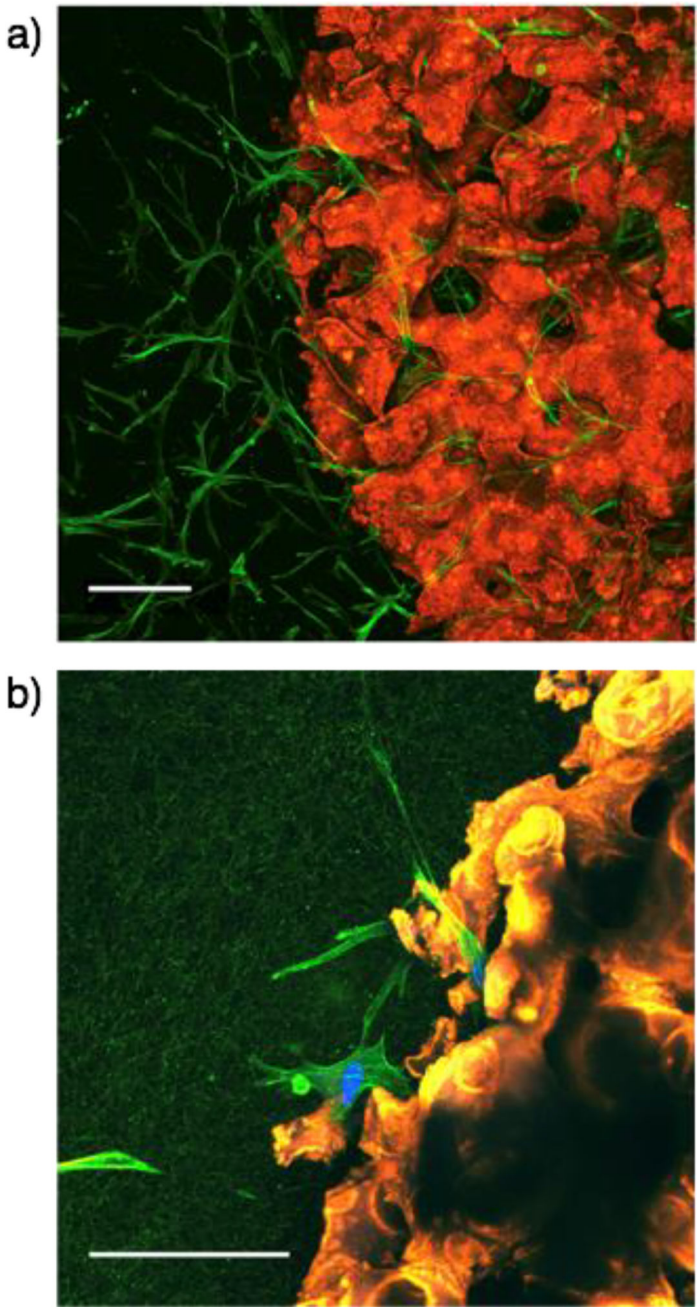

Figure 5.

NHDF delivery to encapsulating fibrin after 8 days. a) Confocal microscopy maximum intensity projection (image stack: 225 μm) of the fibrin-CBiTH interface (Green: AlexaFluor 488 phalloidin labeling of F-actin, Red: RITC-labeled silica nanoparticles, Scale bar: 100 μm). b) Confocal microscopy maximum intensity projection (image stack: 75 μm) of the fibrin-CBiTH interface with added reflection imaging (Blue: DAPI labeling of cell nuclei, Green: reflected light and AlexaFluor 488 phalloidin labeling of F-actin, Orange: combination of the reflected light (green) and RITC-labeled silica nanoparticles (red), Scale bar: 200 μm).

Author Manuscript Author Manuscript Author Manuscript Author Manuscript

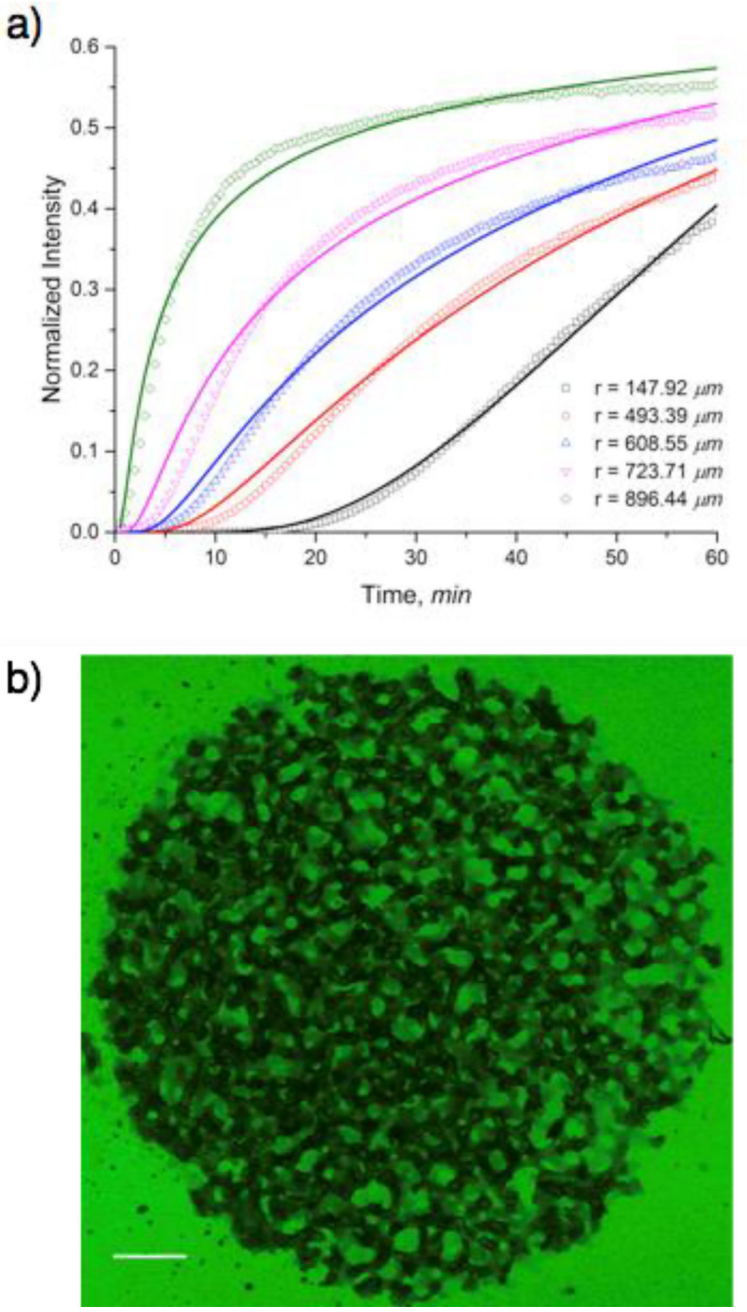

Figure 6.

Dextran diffusion in bijel-templated PEG scaffolds. a) Normalized intensity over time of experimental data (open symbols, n=3) and transient radial diffusion model fits (solid lines) at 5 positions: r=147.92 μm (−), r=493.39 μm (−), r=608.55 μm (−), r=723.71 μm (−), and r=896.44 μm (−). b) Confocal micrograph of scaffold sample after overnight incubation in dextran solution (Green: fluorescein isothiocyanate-dextran, Imaging depth: 60 μm, Scale bar: 250 μm).

Author Manuscript

Author Manuscript

Author Manuscript

Author Manuscript

Table 1

Compressive modulus and strength of cell delivery hydrogels

Sample	Compressive Modulus, E (kPa)	Compressive Strength, σ_u (kPa)
Control PEG	2346.53 ± 10.3%	238.00 ± 3.61%[a]
Bijel-templated PEG	800.67 ± 13.3%[a]	241.33 ± 1.53%[a]
Fibrin-PEG CBiTH	836.07 ± 15.1%[a]	238.33 ± 1.15%[a]

[a] no statistical difference detected between samples ($p > 0.0167$)